

1 **Supplemental Information for**  
2 **Using observed urban NO<sub>x</sub> sinks to constrain VOC reactivity and the ozone and radical**  
3 **budget in the Seoul Metropolitan Area**

4 Benjamin A. Nault<sup>1,2,\*</sup>, Katherine R. Travis<sup>3</sup>, James H. Crawford<sup>3</sup>, Donald R. Blake<sup>4</sup>, Pedro  
5 Campuzano-Jost<sup>5</sup>, Ronald C. Cohen<sup>6</sup>, Joshua P. DiGangi<sup>3</sup>, Glenn S. Diskin<sup>3</sup>, Samuel R. Hall<sup>7</sup>, L.  
6 Gregory Huey<sup>8</sup>, Jose L. Jimenez<sup>5</sup>, Kyung-Eun Kim<sup>9</sup>, Youngro Lee<sup>8,a</sup>, Isobel J. Simpson<sup>4</sup>, Kirk  
7 Ullmann<sup>7</sup>, Armin Wisthaler<sup>10,11</sup>

8 <sup>1</sup>CACC, Aerodyne Research, Inc., Billerica, MA, USA

9 <sup>2</sup>Department of Environmental Health and Engineering, Johns Hopkins University, Baltimore,  
10 MD, USA

11 <sup>3</sup>NASA Langley Research Center, Hampton, VA, USA

12 <sup>4</sup>Department of Chemistry, University of California, Irvine, CA, USA

13 <sup>5</sup>CIRES and Department of Chemistry, University of Colorado, Boulder, CO, USA

14 <sup>6</sup>Department of Chemistry, University of California, Berkeley, CA, USA

15 <sup>7</sup>Atmospheric Chemistry Observations & Modeling Laboratory, NCAR, Boulder, CO, USA

16 <sup>8</sup>School of Earth & Atmospheric Sciences, Georgia Institute of Technology, Atlanta, GA, USA

17 <sup>9</sup>School of Environmental Sciences and Environmental Engineering, Gwangju Institute of Science  
18 and Technology, Gwangju, South Korea

19 <sup>10</sup>University of Oslo, Oslo, Norway

20 <sup>11</sup>University of Innsbruck, Innsbruck, Austria

21  
22 <sup>a</sup>Now at Division of Geological and Planetary Sciences, California Institute of Technology,  
23 Pasadena, CA, USA

24  
25  
26 \*Corresponding author:

27 Email: bnault@aerodyne.com or bnault1@jh.edu

28

29 *For ACP*

30 **S1. Analytical Equation for P(O<sub>x</sub>)**

31 The analytical description of P(O<sub>x</sub>) and impacts from ΣANs chemistry has been described  
 32 elsewhere (Farmer et al., 2011 and references therein). Briefly, P(O<sub>x</sub>) can be described by  
 33 combining the following equations (Eq. S1 – S8). These equations are assumed to describe P(O<sub>x</sub>)  
 34 for a single time during the day and is derived from the assumption that the HO<sub>x</sub> radicals (HO<sub>x</sub> =  
 35 OH + HO<sub>2</sub> + RO<sub>2</sub>) are in photostationary steady-state. The steady-state assumption for HO<sub>x</sub> means  
 36 production and loss are equal.

$$37 \quad P(HO_x) = L(HO_x) = k_{OH+NO_2}[OH][NO_2] + \alpha k_{NO+RO_2}[NO][RO_2] +$$

$$38 \quad 2k_{HO_2+HO_2}[HO_2][HO_2] + 2k_{RO_2+HO_2}[HO_2][RO_2] + 2k_{RO_2+RO_2}[RO_2][RO_2] \quad (\text{Eq. S1})$$

39 As described elsewhere, under the assumption of rapid P(O<sub>x</sub>) and thus radical chain propagation  
 40 dominates, every RO<sub>2</sub> that is produced by the photooxidation of a VOC by OH will react with an  
 41 NO molecule (R2, Sect. 1), and some fraction of the time (e.g., 1 – α, the effective branching ratio),  
 42 produce HO<sub>2</sub> following the reaction of the alkoxy radical (RO) with O<sub>2</sub>. Therefore, it is assumed  
 43 that,

$$44 \quad [HO_2] \approx [RO_2] \approx \frac{k_{OH+VOC}[VOC][OH]}{(1-\alpha)k_{NO+RO_2}[NO]} \quad (\text{Eq. S2})$$

45 Combining Eq. S1 and S2 together with an assumed P(HO<sub>x</sub>), [OH] can be calculated using the  
 46 quadratic formula:

$$47 \quad [OH_{Calc}] = \frac{-b \pm \sqrt{b^2 - 4ac}}{2a} \quad (\text{Eq. S3})$$

48 where

$$49 \quad a = (2k_{HO_2+HO_2} + 2k_{RO_2+HO_2} + 2k_{RO_2+RO_2}) \left( \frac{k_{OH+VOC}[VOC]}{(1-\alpha)k_{NO+RO_2}[NO]} \right)^2 \quad (\text{Eq. S4})$$

$$50 \quad b = k_{OH+NO_2}[NO_2] + \frac{\alpha k_{NO+RO_2}}{(1-\alpha)k_{NO+RO_2}} \quad (\text{Eq. S5})$$

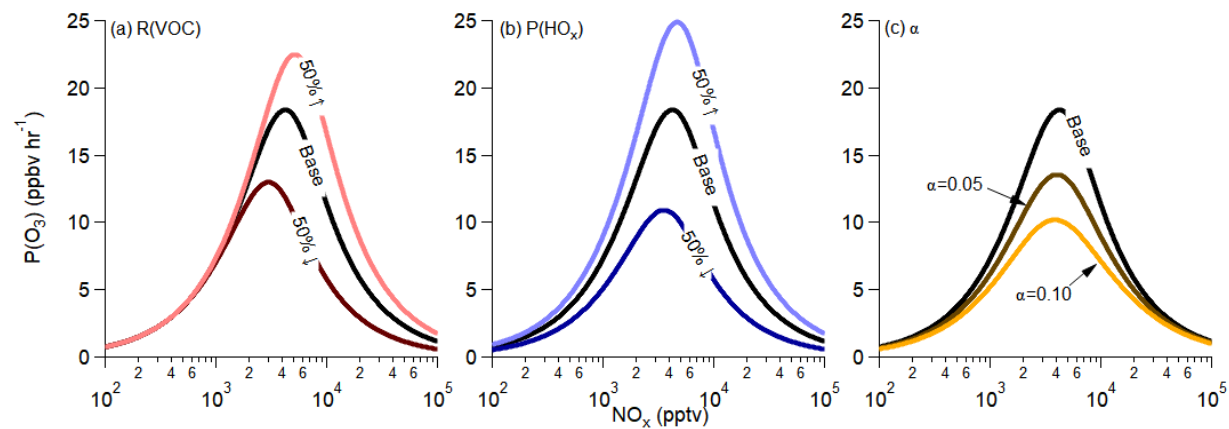
$$51 \quad c = -P(HO_x) \quad (\text{Eq. S6})$$

52 In the above equations,  $k$  is the rate constant for the described reaction in the subtext (e.g.,  $\text{HO}_2 +$   
53  $\text{HO}_2$ ), the term  $k_{\text{OH}+\text{VOC}}[\text{VOC}]$  can be simplified to the VOC reactivity ( $R(\text{VOC})$ ,  $\text{s}^{-1}$ ) for the  
54 ambient mixture of VOCs,  $\alpha$  is the effective branching ratio for the ambient mixture of VOCs, and  
55  $P(\text{HO}_x)$  is the  $\text{HO}_x$  production rate for the ambient mixture of gases. The rate constants for the two  
56  $\text{HO}_x$  self-reactions,  $\text{HO}_2$  ( $k_{\text{HO}_2+\text{HO}_2}$ ) and  $\text{RO}_2$  ( $k_{\text{RO}_2+\text{RO}_2}$ ), and the  $\text{HO}_2$ - $\text{RO}_2$  reaction ( $k_{\text{HO}_2+\text{RO}_2}$ )  
57 were taken from Sander et al. (2011) for temperatures at 298 K and are  $1.4 \times 10^{-12}$ ,  $6.8 \times 10^{-14}$ , and  
58  $8 \times 10^{-12} \text{ cm}^3 \text{ molec.}^{-1} \text{ s}^{-1}$ , respectively. The OH and  $\text{NO}_2$  rate constant is also from Sander et al.  
59 (2011) for temperatures at 298 K and is  $1.2 \times 10^{-11} \text{ cm}^3 \text{ molec.}^{-1} \text{ s}^{-1}$ . For the base case used here,  
60  $P(\text{HO}_x)$  is assumed to be  $1 \times 10^7 \text{ molec. cm}^{-3} \text{ s}^{-1}$ ,  $\alpha$  is 0, and  $R(\text{VOC})$  ( $k_{\text{OH}+\text{VOC}}[\text{VOC}]$ ) is  $5.00 \text{ s}^{-1}$ .  
61 Finally, the instantaneous  $P(\text{O}_x)$  can be approximated as

$$62 \quad P(\text{O}_x) = k_{\text{HO}_2+\text{NO}}[\text{HO}_2][\text{NO}] + (1 - \alpha)k_{\text{RO}_2+\text{NO}}[\text{RO}_2][\text{NO}] \quad (\text{Eq. S7})$$

$$63 \quad P(\text{O}_x) = 2(1 - \alpha)k_{\text{OH}+\text{VOC}}[\text{VOC}][\text{OH}_{\text{Calc}}] \quad (\text{Eq. S8})$$

64



65

66 **Figure S1.** Example analytical solutions to instantaneous  $P(O_x)$ , assuming different scenarios with  
 67 changes in total VOC reactivity ( $R(\text{VOC})$ ) (a), changes in  $\text{HO}_x$  radical production ( $P(\text{HO}_x)$ ) (b), or  
 68 changes in the alkyl and multi-functional nitrate effective branching ratio ( $\alpha$ ) (c). See Sect. S1 and  
 69 Eq. S1 – S8 for the analytical equations.

70 **Table S1.** Measured VOCs and their associated MCMv3.3.1 species in F0AM.

MCMv3.3.1 species	Aircraft observation
CH3CHO	Acetaldehyde (PTRMS)
CH3COCH3	Acetone (PTRMS)
BENZENE	Benzene (PTRMS)
TOLUENE	Toluene (PTRMS)
MXYL	C8 alkylbenzenes (PTRMS)*20% <sup>1,2</sup>
PXYLE	C8 alkylbenzenes (PTRMS)*20% <sup>1,2</sup>
OXYLE	C8 alkylbenzenes (PTRMS)*17% <sup>1</sup>
STYRENE	C8 alkylbenzenes (PTRMS)*2% <sup>1</sup>
EBENZ	C8 alkylbenzenes (PTRMS)*41% <sup>1</sup>
C2H4	Ethene (WAS)
C2H2	Ethyne (WAS)
C2H6	Ethane (WAS)
C5H8	Isoprene (WAS)
IC4H10	i-Butane (WAS)
NC4H10	n-Butane (WAS)
IC5H12	i-Pentane (WAS)
NC5H12	n-Pentane (WAS)
PBENZ	i-Propylbenzene + n-Propylbenzene (WAS)
MEK	MEK (PTRMS)
CH3OH	Methanol (PTRMS)
C2H5OH	Methanol/2.5 <sup>3</sup>
NC7H16	n-Heptane (WAS)
NC10H22	n-Decane (WAS)
NC6H14	n-Hexane (WAS)
NC8H18	n-Octane (WAS)
C3H8	Propane (WAS)
C3H6	Propene (WAS)
C4H6	1,3-Butadiene (WAS)
OETHTOL	2-Ethyltoluene (WAS)
METHTOL	3-Ethyltoluene (WAS)
PETHTOL	4-Ethyltoluene (WAS)
TM123B	1,2,3-Trimethylbenzene (WAS)
TM124B	1,2,4-Trimethylbenzene (WAS)
TM135B	1,3,5-Trimethylbenzene (WAS)
BPINENE	Monoterpenes (PTRMS)*0.45 <sup>1</sup>
APINENE	Monoterpenes (PTRMS)*0.55 <sup>1</sup>

71 <sup>1</sup>Speciated based on WAS measurements.72 <sup>2</sup>Assume 50/50 split m-xylene vs. p-xylene.73 <sup>3</sup>According to Schroeder et al. (2020)

74 **Table S2.** The higher PNs lumping based on their primary precursor species from F0AM.

<b>Lumped PN</b>	<b>Primary Precursors</b>	<b>Largest PN in MCMv3.3.1</b>
Arom	Aromatics: benzene, toluene, xylenes, ethylbenzene, propylbenzene, ethyltoluene, trimethylbenzenes, styrene	ACCOMEPAN
Alk	MEK, butane, pentane, decane, etc.	C3PAN1
Isop	Isoprene	CO2C3PAN
Monoterpenes	Monoterpenes	C3PAN2

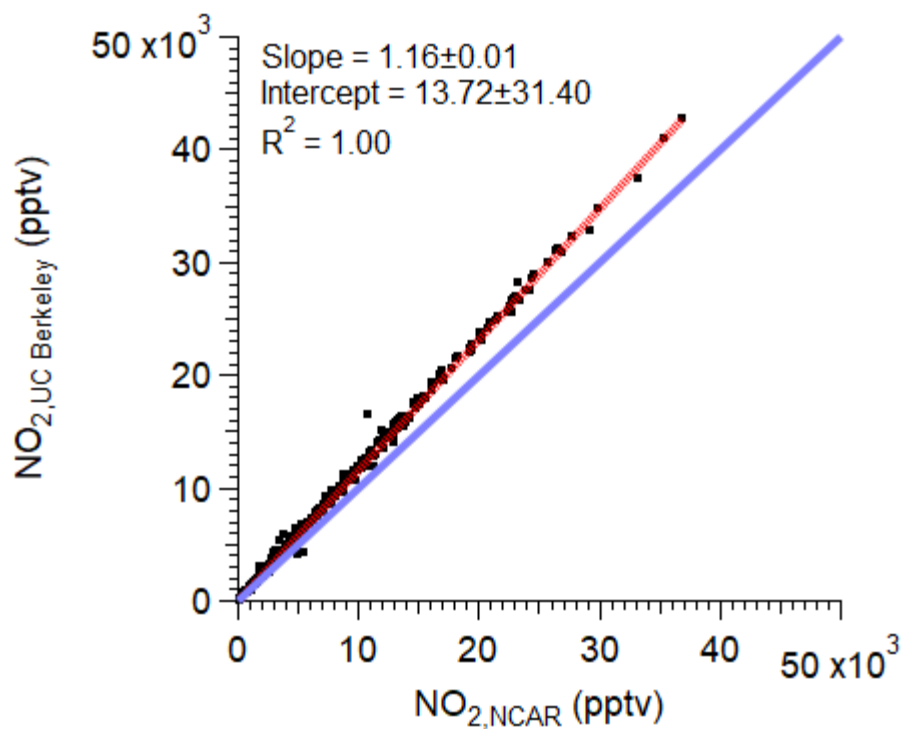
75

## 76 S2. Comparison of NO<sub>2</sub> Measurements

77 There were three different measurements of NO<sub>2</sub> on the DC-8 during KORUS-AQ: (1) by  
78 chemiluminescence (Weinheimer et al., 1994), (2) by laser induced fluorescence (Thornton et al.,  
79 2000), and (3) by cavity enhanced absorption spectroscopy (Min et al., 2016). Here, only  
80 chemiluminescence and laser induced fluorescence are considered. Comparison of the NO<sub>2</sub> mixing  
81 ratios by these two measurements are shown in Figure S2. Though the correlation is high ( $R^2 =$   
82 1.00), the laser induced fluorescence NO<sub>2</sub> is ~16% higher than the chemiluminescence NO<sub>2</sub>. To  
83 determine which NO<sub>2</sub> to use for the study, the NO<sub>2</sub>-to-NO ratio was compared, as this ratio can be  
84 calculated with the observations on the DC-8. This ratio is defined by Eq. S9:

$$85 \quad \frac{[\text{NO}_2]}{[\text{NO}]} = \frac{k_{\text{NO}+\text{O}_3}[\text{O}_3] + k_{\text{NO}+\text{HO}_2}[\text{HO}_2] + k_{\text{NO}+\text{RO}_2}[\text{RO}_2]}{j_{\text{NO}_2}} \quad (\text{Eq. S9})$$

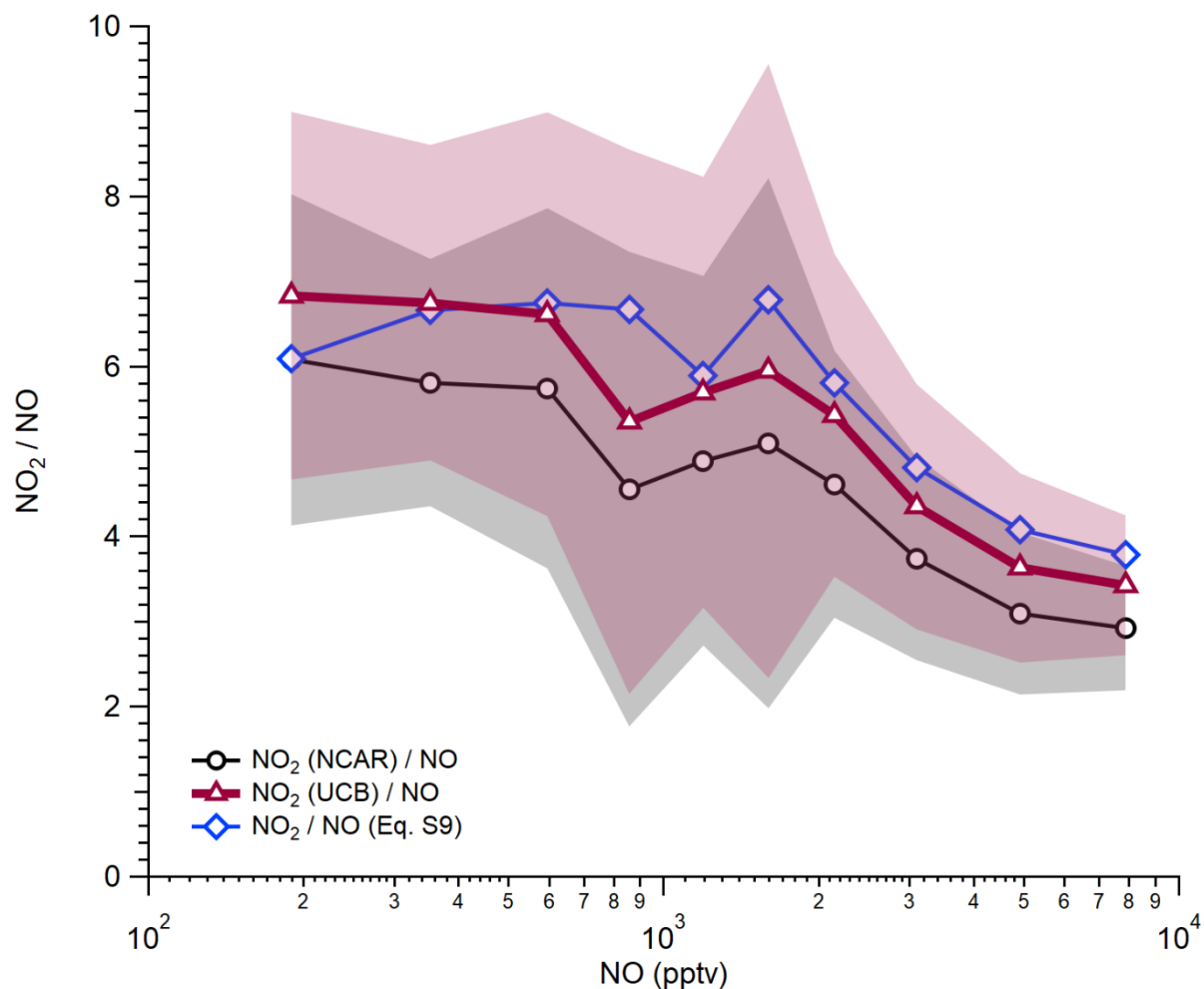
86 Note, though steady-state RO<sub>2</sub> is used throughout the paper and can provide some uncertainty in  
87 the calculated NO<sub>2</sub>-to-NO ratio in Eq. S9, at high NO mixing ratios where both HO<sub>2</sub> and RO<sub>2</sub>  
88 concentrations are low, the O<sub>3</sub> + NO reaction dominates the term. It was found that the NO<sub>2</sub>-to-  
89 NO ratio using the University of California, Berkeley, NO<sub>2</sub> generally agreed better with the  
90 calculated NO<sub>2</sub>-to-NO ratio from Eq. S9. However, both NO<sub>2</sub>-to-NO ratios 1 $\sigma$  spread of  
91 observations overlap with the calculated NO<sub>2</sub>-to-NO ratio from Eq. S9. Thus, the University of  
92 California, Berkeley, NO<sub>2</sub> measurements are used throughout the manuscript. The use of the  
93 NCAR NO<sub>2</sub> had small changes but does not change the main conclusions and trends discussed  
94 throughout the paper.



95

96 **Figure S2.** Scatter plot of the NO<sub>2</sub> measured by University of California, Berkeley, laser induced  
97 fluorescence and the NCAR chemiluminescence. The one-to-one line is shown in blue and the  
98 ODR fit for the data is shown in red.





99

100 **Figure S3.** Binned NO<sub>2</sub>-to-NO ratio, where NO is from NCAR chemiluminescence and NO<sub>2</sub> is  
 101 either from NO<sub>2</sub> chemiluminescence (black) or University of California, Berkeley, laser induced  
 102 fluorescence (dark red), versus NO. Shading is ±1σ spread in the observations for both observed  
 103 ratios. The NO<sub>2</sub>-to-NO ratio in blue is calculated using observations (Table 2) and Eq. S9.

### 104 S3. Error Analysis in Calculation of $\alpha_{\text{eff}}$ and R(VOC)

105 In Sect. 3.3, Eq. 8 – 11 assumes that  $L(\text{O}_x)$  and  $L(\Sigma\text{ANs})$  is negligible. However,  $L(\text{O}_x)$  is  
106 approximately 25% of the  $P(\text{O}_x)$  over SMA (e.g., Figure 6). An analysis of how much unmeasured  
107 R(VOC) and the  $\alpha_{\text{eff}}$  is impacted by neglecting these two terms is calculated using Eq. S9.

$$108 \quad \frac{\Delta\text{O}_x}{\Delta\Sigma\text{ANs}} \approx \frac{P_{\text{O}_x}}{P\Sigma\text{ANs}} = \frac{\gamma(1-\alpha)R(\text{VOC})[\text{OH}] - L(\text{O}_x)}{\alpha R(\text{VOC})[\text{OH}] - L(\Sigma\text{ANs})} \quad (\text{Eq. S9})$$

109 Here,  $\gamma$  is the effective  $\text{O}_x$  produced per VOC reacted (1.53),  $\alpha$  is the effective branching ratio to  
110 form  $\Sigma\text{ANs}$ ,  $R(\text{VOC})$  is the VOC and CO reactivity, and  $L_{\text{O}_x}$  and  $L_{\Sigma\text{ANs}}$  are the loss terms for  $\text{O}_x$   
111 and  $\Sigma\text{ANs}$ .

112 One limit in these equations is if  $L(\Sigma\text{ANs})$  is near 0 and  $L(\text{O}_x)$  is important. At this limit,  
113 assuming all R(VOC) is captured by observations, this would lead to an  $\alpha_{\text{eff}}$  of  $\sim 0.02$ . This is  
114 equivalent to the calculated  $\alpha_{\text{eff}}$  using the observed VOCs and calculated secondary VOCs from  
115 F0AM and would indicate no missing R(VOCs).

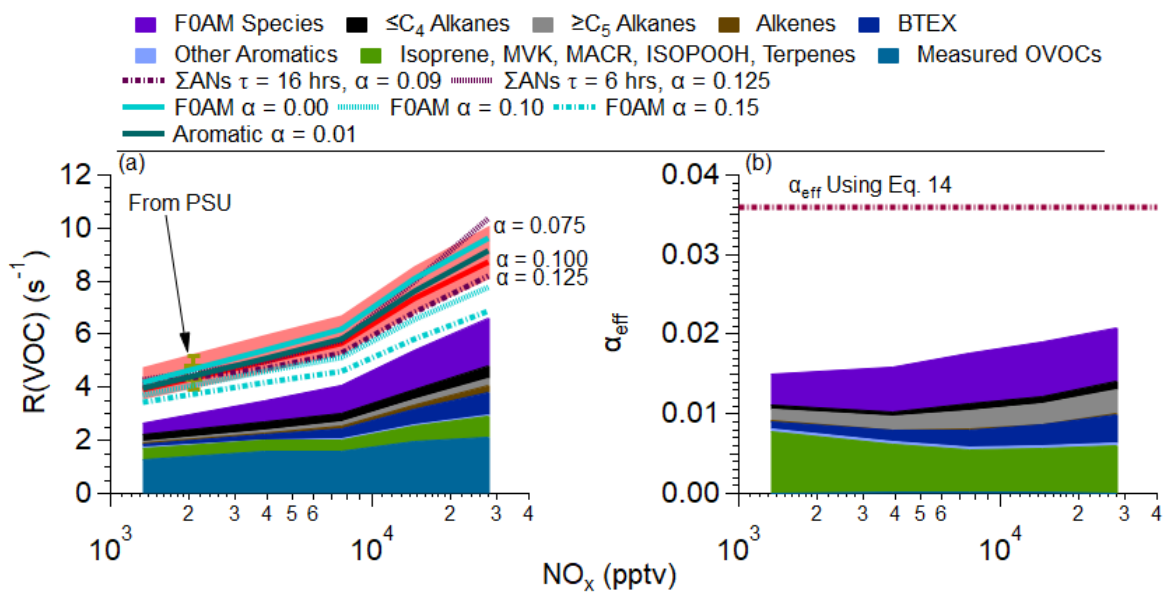
116 However, there are multiple reasons to assume this limit in that  $L(\Sigma\text{ANs})$  is 0 is incorrect  
117 and that the observations do not capture  $\alpha_{\text{eff}}$  and R(VOC). First, the total OH reactivity measured  
118 by Penn State indicates missing reactivity at low  $\text{NO}_x$  mixing ratios, as discussed in Sect. 3.3 and  
119 shown in Fig. 4. Second, the comparison of speciated and measured  $\Sigma\text{PNs}$  as well as the  
120 comparison of the F0AM calculated and measured  $\Sigma\text{PNs}$  indicates missing R(VOC) to account  
121 for the unmeasured PNs, as discussed in Sect. 3.1 and 3.4 and Fig. 2 and 5. Finally, González-  
122 Sánchez et al. (2023) showed that even for long-lived ANs, the lifetime is  $\sim 50$  hours. However,  
123 for multifunctional ANs, this lifetime drops down to 2 – 16 hours. Note, however these  
124 multifunctional ANs are mainly from biogenic VOCs and not anthropogenic VOCs. Yet, as  
125 predicted in MCM (Jenkin et al., 2015), ANs from anthropogenic VOCs are expected to have  
126 similar lifetimes as ANs from biogenic VOCs.

127 To investigate the role of  $L(\sum\text{ANs})$  and  $L(\text{O}_x)$  on unmeasured  $R(\text{VOC})$  and  $\alpha$ , Eq. S9  
128 instead of Eq. 11 is used. The results are summarized in Figure S4. If the ANs lifetime of 16 hours  
129 is assumed, which may be a lower limit, the average unmeasured  $R(\text{VOC})$  decreases from  $1.7_{-0.4}^{+1.1}\text{s}^{-1}$   
130  $^1$  to  $1.4\text{ s}^{-1}$ , and the unmeasured  $\alpha$  would be 0.09, leading to an  $\alpha_{\text{eff}}$  of 0.032. Note, both of these  
131 values are very close to the values calculated assuming losses were negligible. For the unmeasured  
132  $R(\text{VOC})$  and  $\alpha$  shown in Fig. 4, the  $\sum\text{ANs}$  lifetime would be equivalent to 11.5 hrs. This is in the  
133 range of lifetime for multifunctional ANs, but a lower limit (González-Sánchez et al., 2023). If the  
134 typical ANs lifetime shown in González-Sánchez et al. (2023),  $\sim 6$  hrs, is assumed, the average  
135 unmeasured  $R(\text{VOC})$  increases from  $1.7_{-0.4}^{+1.1}\text{ s}^{-1}$  to  $2.2\text{ s}^{-1}$ . This would lead to an  $\alpha_{\text{eff}}$  of 0.045. Note  
136 this is still with the uncertainty of  $R(\text{VOC})$  found with the Penn State observations at low  $\text{NO}_x$ .  
137 Thus, though uncertainty in both  $\sum\text{ANs}$  lifetime and the unmeasured  $\alpha$  impact the calculated  
138 unmeasured  $R(\text{VOC})$ , (a) inclusion of the loss terms of both  $\text{O}_x$  and  $\sum\text{ANs}$  lies within the spread in  
139 observed  $R(\text{VOC})$  at low  $\text{NO}_x$  mixing ratios and the associated calculated  $R(\text{VOC})$  assuming the loss  
140 terms were negligible, (b) if the  $L(\text{O}_x)$  term is considered, the  $L(\sum\text{ANs})$  term must also be included  
141 as it is non-negligible in environments with freshly-produced, multifunctional ANs.

142 There are two potential other sources of uncertainty in the calculated, unmeasured  
143  $R(\text{VOC})$ —(1) assumed  $\alpha$  for the F0AM secondary species and (2)  $\alpha$  for aromatics. First, for  $\alpha$   
144 ranging from 0.00 – 0.10 for F0AM species, the unmeasured  $R(\text{VOC})$  falls within the spread of  
145 observations and calculated unmeasured  $R(\text{VOC})$  assuming F0AM  $\alpha$  is 0.05. Thus, the calculated  
146 unmeasured is insensitive to the F0AM  $\alpha$  until the F0AM  $\alpha$  is greater than 0.10. Though the  $\alpha$   
147 values for secondary, oxygenated species is unconstrained (Orlando and Tyndall, 2012),  $\alpha$  being  
148 greater than 0.10 is currently unexpected with what is currently known about chemistry of these  
149 secondary species. Second, the  $\alpha$  for aromatic compounds was changed from the values found in

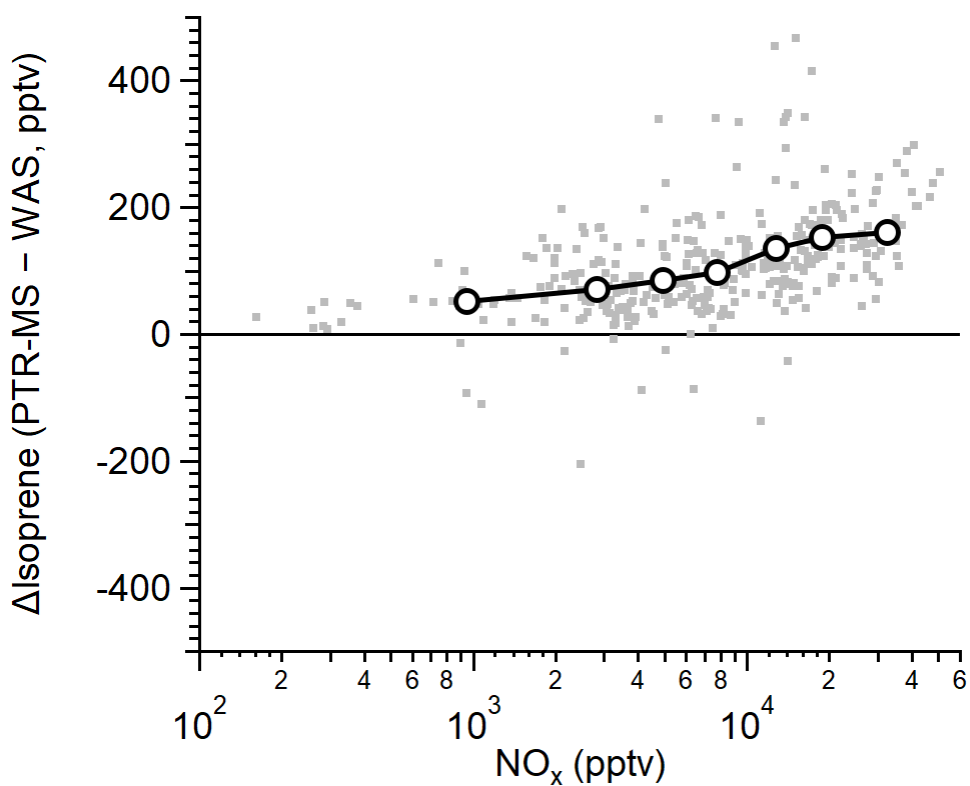
150 MCM (Jenkin et al., 2015) and Perring et al. (2013) to all being 0.01. This is due to recent a recent  
151 study finding that  $\alpha$  is potentially lower for aromatic compounds (Xu et al., 2020). Even with this  
152 low  $\alpha$  value for the aromatics, the average unmeasured RVOC is not greatly impacted, increasing  
153 from 1.7 to 1.8 s<sup>-1</sup>. This is due to the aromatics accounting for a small fraction of the total  $\alpha$  and  
154  $\sum$ ANs.

155 Thus, though there are numerous assumptions and sources of uncertainty associated with  
156 constraining the unmeasured RVOC with the observations, the overall results of, on average, 1.7  
157 s<sup>-1</sup> unmeasured RVOC is robust. As these various sensitivity investigations minimally impact the  
158 calculated unmeasured RVOCs using the assumptions in the main text, the unmeasured RVOCs  
159 associated with  $\alpha = 0.10$  and assuming the loss terms are negligible are used.



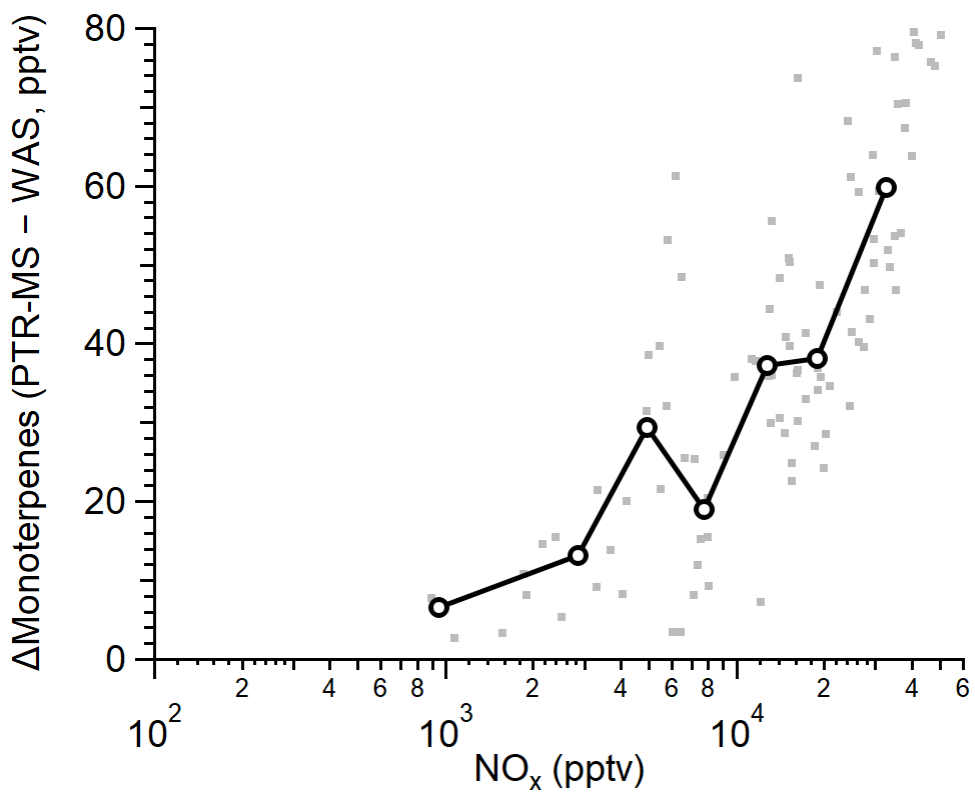
160

161 **Figure S4.** Same as Figure 4, but with the sensitivities discussed in Sect. S3, including inclusion  
 162 of  $\text{O}_x$  and ANs loss terms, range of  $\alpha$  for F0AM secondary species, and lowering the aromatic  $\alpha$   
 163 value.



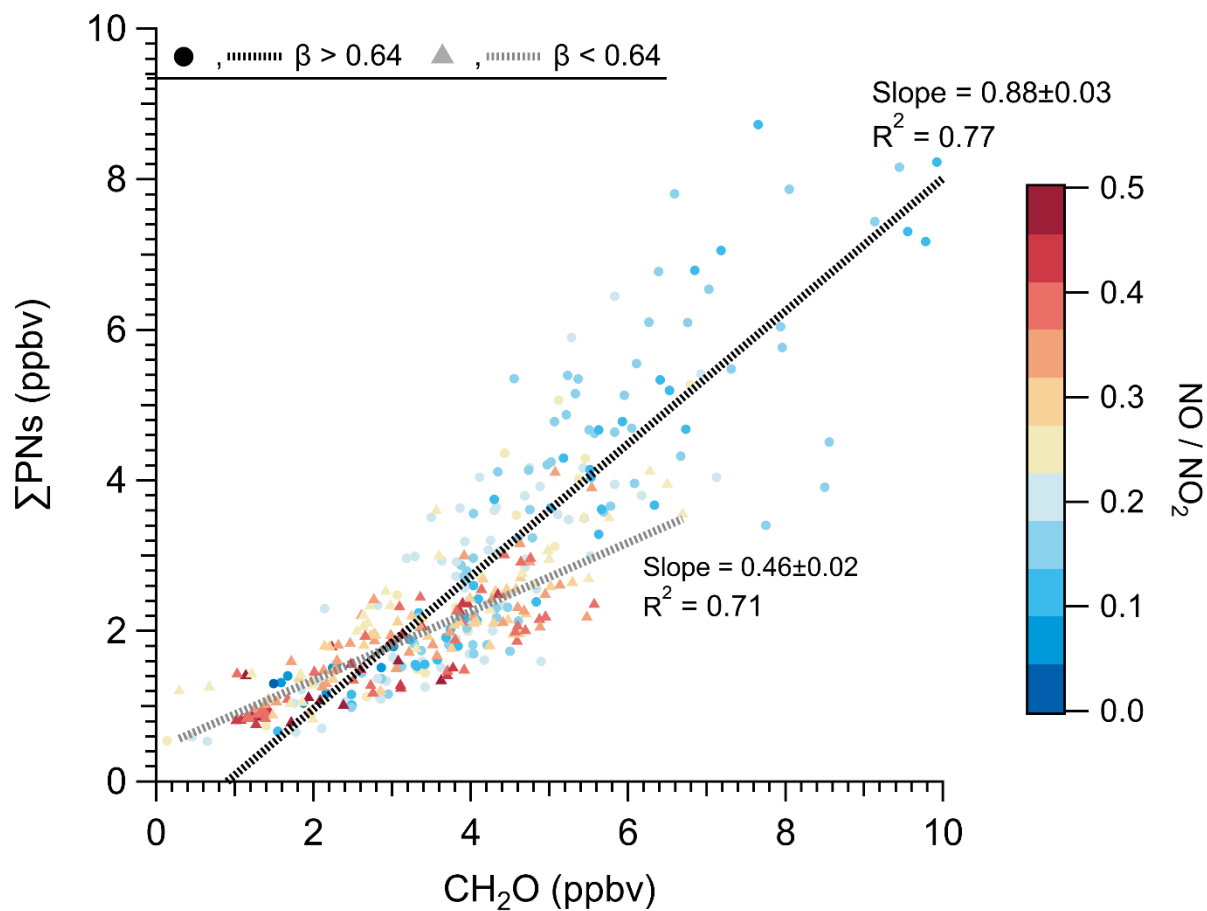
164

165 **Figure S5.** The difference in the isoprene mixing ratio measured by University of Oslo PTR-MS  
 166 and University of California, Irvine WAS, versus the observed NO<sub>x</sub>. All data are shown in grey  
 167 and equally sized bins are shown in black for observations collected over the SMA.



168

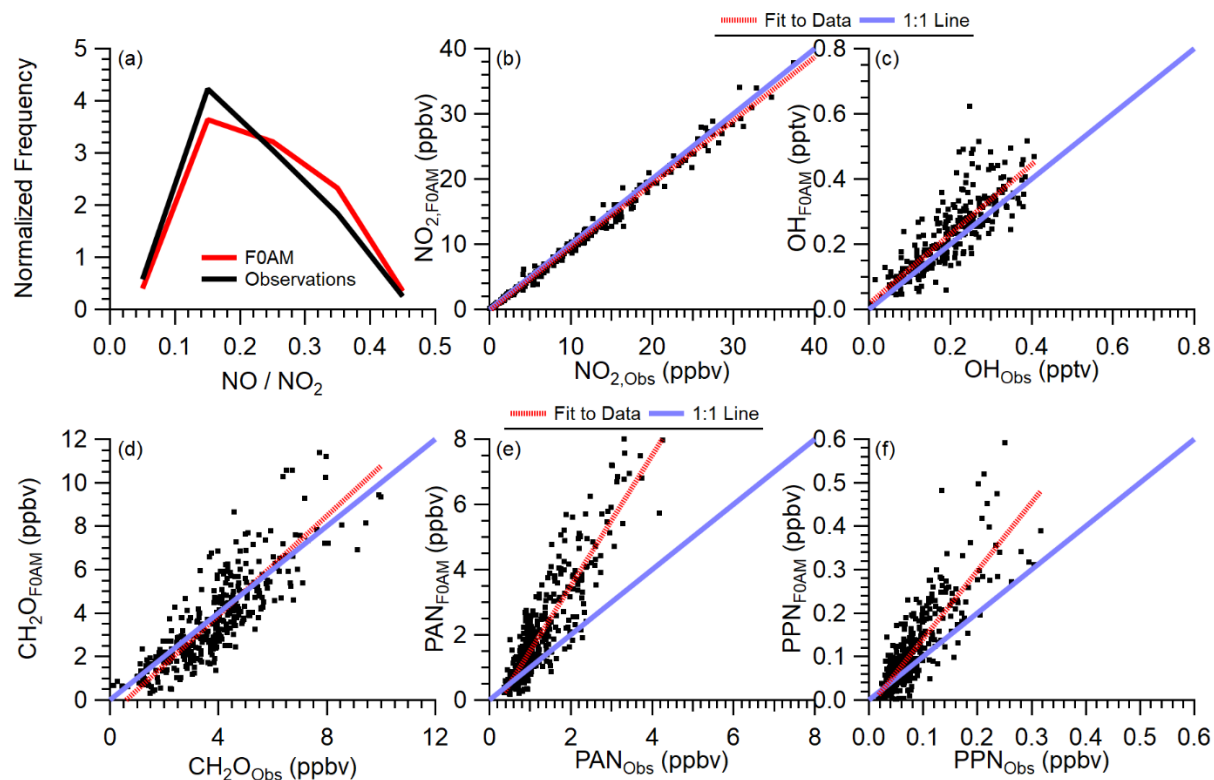
169 **Figure S6.** Same as Figure S5, but for monoterpenes. Lower amount of data is associated with the  
 170 measurements being below detection limit for WAS.



171

172 **Figure S7.** Same as Figure 3b, but with the data colored by the NO-to-NO<sub>2</sub> ratio. Further, the fits  
 173 are differentiated between the  $\beta$  value, where  $\beta$  value describes the fraction of time an acyl peroxy  
 174 radical (R(O)O<sub>2</sub>) reacts with NO<sub>2</sub> versus NO. The  $\beta$  is equal to  $(k_{R(O)O_2+NO_2}[NO_2]) / (k_{R(O)O_2+NO_2}[NO_2] + k_{R(O)O_2+NO}[NO])$ .  
 175





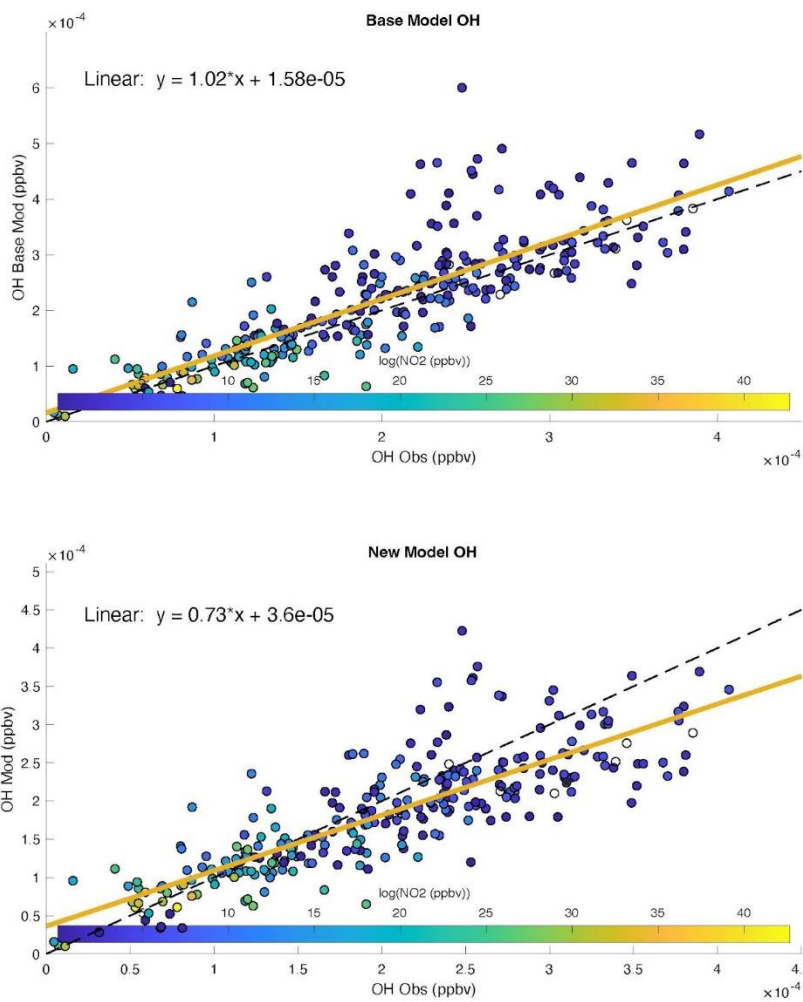
176

177 **Figure S8.** Evaluation of the F0AM model performance versus gases measured on DC-8 over the  
 178 SMA and not used to constrain the model. (a) Normalized frequency of the NO-to-NO<sub>2</sub> ratio  
 179 predicted by F0AM and measured (NCAR NO and UC Berkeley NO<sub>2</sub>). (b) Scatter plot of F0AM  
 180 predicted NO<sub>2</sub> versus observed NO<sub>2</sub> from UC Berkeley. (c) Scatter plot of F0AM predicted OH  
 181 versus Penn State observed OH. (d) Scatter plot of F0AM predicted CH<sub>2</sub>O versus CAMS observed  
 182 CH<sub>2</sub>O. (e) Scatter plot of F0AM predicted PAN versus GT-CIMS observed PAN. (f) Scatter plot  
 183 of F0AM predicted PPN versus GT-CIMS observed PPN.

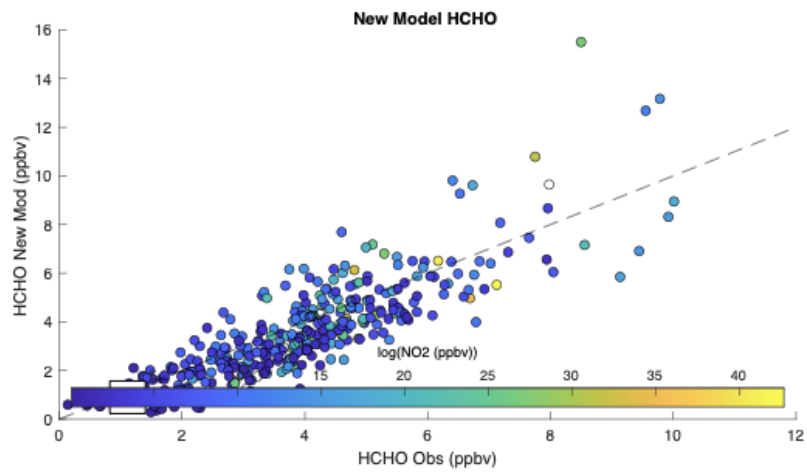
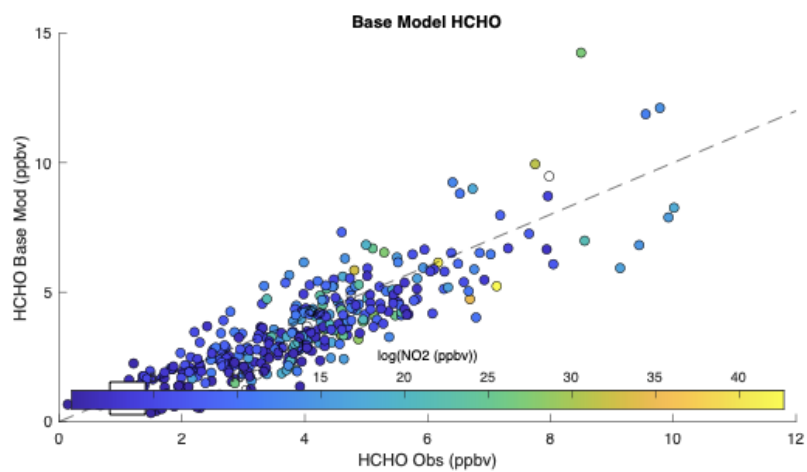
#### 184 **S4. Sensitivity in F0AM Results with Missing R(VOC)**

185 We add to the model a test of whether the estimated additional OH reactivity of  $\sim 1.7 \text{ s}^{-1}$   
186 would degrade model performance in simulating formaldehyde or OH. We add approximately 800  
187 pptv of  $\text{C}_4\text{H}_9\text{CHO}$  (pentanal), on average, as a proxy for unmeasured aldehydes, such as octanal,  
188 nonanal, decanal, etc. The concentration of pentanal varies according to the calculated missing OH  
189 reactivity. The average OH reactivity from this species is  $\sim 0.5 \text{ s}^{-1}$ . Total OH reactivity goes up by  
190  $1.2 \text{ s}^{-1}$  after including all the products produced from the oxidation of pentanal. Therefore, the  
191 added primary species (pentanal) results in over twice as much reactivity from secondary oxidation  
192 products. The largest secondary oxidation products are smaller aldehydes ( $\text{HOC}_3\text{H}_6\text{CHO}$ ,  
193  $\text{HOC}_2\text{H}_4\text{CHO}$ ,  $\text{C}_3\text{H}_7\text{CHO}$ ), which have OH reactivity of 0.1 to  $0.2 \text{ s}^{-1}$  each. With the inclusion of  
194  $\sim 0.5 \text{ s}^{-1}$  pentanal to F0AM as a surrogate for missing R(VOC), OH is reduced by  $\sim 25\%$  compared  
195 to the base model (Figure S9). We attribute this OH reduction to the build-up of the peroxyxynitrate  
196 ( $\text{C}_5\text{H}_9\text{NO}_5$ ) from pentanal to approximately 500 pptv. This pentanal peroxyxynitrate is likely  
197 overestimated given the rapid exposure of PN species to warmer temperatures through mixing, as  
198 discussed by Crawford et al. (2021). Model formaldehyde change with the inclusion of  $\sim 0.5 \text{ s}^{-1}$   
199 pentanal to F0AM by  $< 5\%$  (Figure S10). This is attributed to the balance of increased production  
200 of formaldehyde and  $\text{RO}_2$  to convert NO to  $\text{NO}_2$  by pentanal, but the decreased OH which then  
201 reduces production/conversion.

202



203  
 204 **Figure S9.** Comparison of F0AM predicted OH versus observed OH for the base F0AM model  
 205 (top) and sensitivity F0AM model that included  $\sim 0.5 \text{ s}^{-1}$  pentanal to account for missing R(VOC).  
 206 The values are colored by observed  $\text{NO}_2$  (note, the scale is in logarithmic scale).  
 207



208

209 **Figure S10.** Same as Figure S9, except for formaldehyde.

210

#### 211 **S4. Aerosol Contamination of the CAFS Downwelling Optic**

212           During KORUS-AQ ambient aerosols deposits were regularly evident on all leading edges  
213 of the aircraft, particularly during low altitude spirals near Seoul. The deposits collected on the  
214 leading edge of the downwelling CAFS optic (Figure S9), resulting in optical reductions in the  
215 actinic flux of up to 20%. The precise reductions depended on the aerosol coating efficiency and  
216 cleaning by precipitation. The optic was centered above the DC-8 fuselage in the zenith 1 port,  
217 just aft of the forward cabin exit door. The upwelling optic was unaffected, likely due to the larger  
218 aircraft boundary layer near its location under the aft fuselage.

219           Extensive analysis was required to correct the downwelling data. This involved  
220 identification of contaminated periods, characterization of the angular impact, optical thickness  
221 and time evolution. Corrections were applied to the direct beam only. Corrections to diffuse light  
222 were estimated to be small (<3%) and the corrective skill insufficient for application to the data.  
223 Such aerosol coating had not been detected during numerous high aerosol encounters on previous  
224 campaigns. They appear to result from unprecedented aerosol combinations in the SMA.

225           The final CAFS dataset includes a flagging scheme (Table S3) to tag the contaminated  
226 periods. For any quality flag  $> 0$  the photolysis frequency uncertainties should be increased by  
227 20% to account for the low bias during contamination. For quality flag 0 the uncertainty should be  
228 conservatively increased by 10% due to the uncertainty in the aerosol cleaning efficiency during  
229 the remainder of the flights.

230

231 **Table S3.** CAFS data quality flag summary

<b>Quality Flag</b>	<b>Aerosol deposit Contamination?</b>	<b>Direct Beam Impacted?</b>	<b>Correction Applied?</b>	<b>Correction Source</b>
0	No	No	No	-
1	Yes	No	No	-
2	Yes	Yes	Yes	Current spiral
3	Yes	Yes	Yes	Nearest spiral and turns
4	Yes	Unknown	No	Insufficient spiral data

232

233



234

235 **Figure S11.** Strong aerosol contamination of the optic following the flight on 19 May, 2016.

236

237 **References**

- 238 Crawford, J. H., Ahn, J. Y., Al-Saadi, J., Chang, L., Emmons, L. K., Kim, J., Lee, G., Park, J. H.,  
239 Park, R. J., Woo, J. H., Song, C. K., Hong, J. H., Hong, Y. D., Lefer, B. L., Lee, M., Lee, T., Kim,  
240 S., Min, K. E., Yum, S. S., Shin, H. J., Kim, Y. W., Choi, J. S., Park, J. S., Szykman, J. J., Long,  
241 R. W., Jordan, C. E., Simpson, I. J., Fried, A., Dibb, J. E., Cho, S. Y., and Kim, Y. P.: The Korea-  
242 United States air quality (KORUS-AQ) field study, *Elementa*, 9, 1–27,  
243 <https://doi.org/10.1525/elementa.2020.00163>, 2021.
- 244 Farmer, D. K., Perring, A. E., Wooldridge, P. J., Blake, D. R., Baker, A., Meinardi, S., Huey, L.  
245 G., Tanner, D., Vargas, O., and Cohen, R. C.: Impact of organic nitrates on urban ozone  
246 production, *Atmos Chem Phys*, 11, 4085–4094, <https://doi.org/10.5194/acp-11-4085-2011>, 2011.
- 247 González-Sánchez, J. M., Brun, N., Wu, J., Ravier, S., and Clément, J.: On the importance of  
248 multiphase photolysis of organic nitrates on their global atmospheric removal, *Atmos Chem Phys*,  
249 23, 5851–5866, <https://doi.org/10.5194/acp-23-5851-2023>, 2023.
- 250 Jenkin, M. E., Young, J. C., and Rickard, A. R.: The MCM v3.3.1 degradation scheme for isoprene,  
251 *Atmos Chem Phys*, 15, 11433–11459, <https://doi.org/10.5194/acp-15-11433-2015>, 2015.
- 252 Min, K.-E., Washenfelder, R. a., Dubé, W. P., Langford, a. O., Edwards, P. M., Zarzana, K. J.,  
253 Stutz, J., Lu, K., Rohrer, F., Zhang, Y., and Brown, S. S.: A broadband cavity enhanced absorption  
254 spectrometer for aircraft measurements of glyoxal, methylglyoxal, nitrous acid, nitrogen dioxide,  
255 and water vapor, *Atmos Meas Tech*, 9, 423–440, <https://doi.org/10.5194/amt-9-423-2016>, 2016.
- 256 Orlando, J. J. and Tyndall, G. S.: Laboratory studies of organic peroxy radical chemistry: an  
257 overview with emphasis on recent issues of atmospheric significance, *Chem Soc Rev*, 41, 6294–  
258 6317, <https://doi.org/10.1039/c2cs35166h>, 2012.
- 259 Perring, A. E., Pusede, S. E., and Cohen, R. C.: An observational perspective on the atmospheric  
260 impacts of alkyl and multifunctional nitrates on ozone and secondary organic aerosol., *Chem Rev*,  
261 113, 5848–70, <https://doi.org/10.1021/cr300520x>, 2013.
- 262 Sander, S. P., Abbatt, J. P. D., Barker, J. R., Burkholder, J. B., Friedl, R. R., Golden, D. M., Huie,  
263 R. E., Kolb, C. E., Kurylo, M. J., Moortgat, G. K., Orkin, V. L., and Wine, P. H.: Chemical Kinetics  
264 and Photochemical Data for Use in Atmospheric Studies, Evaluation No. 17, JPL Publication 10-  
265 6, Jet Propulsion Laboratory, Pasadena, 2011.
- 266 Schroeder, J. R., Crawford, J. H., Ahn, J. Y., Chang, L., Fried, A., Walega, J., Weinheimer, A.,  
267 Montzka, D. D., Hall, S. R., Ullmann, K., Wisthaler, A., Mikoviny, T., Chen, G., Blake, D. R.,  
268 Blake, N. J., Hughes, S. C., Meinardi, S., Diskin, G., Digangi, J. P., Choi, Y., Pusede, S. E., Huey,  
269 G. L., Tanner, D. J., Kim, M., and Wennberg, P.: Observation-based modeling of ozone chemistry  
270 in the Seoul metropolitan area during the Korea-United States Air Quality Study (KORUS-AQ),  
271 *Elementa*, 8, <https://doi.org/10.1525/elementa.400>, 2020.
- 272 Thornton, J. A., Wooldridge, P. J., and Cohen, R. C.: Atmospheric NO<sub>2</sub>: In-situ laser-induced  
273 fluorescence detection at parts per trillion mixing ratios, *Anal Chem*, 72, 528–539,  
274 <https://doi.org/doi:10.1021/ac9908905>, 2000.
- 275 Weinheimer, A. J., Walega, J. G., Ridley, B. A., Gary, B. L., Blake, D. R., Blake, N. J., Rowland,  
276 F. S., Sachse, G. W., Anderson, B. E., and Collins, J. E.: Meridional distributions of NO<sub>x</sub>, NO<sub>y</sub>,  
277 and other species in the lower stratosphere and upper troposphere during AASE II, *Geophys Res*  
278 *Lett*, 21, 2583–2586, <https://doi.org/10.1029/94GL01897>, 1994.

279 Xu, L., Møller, K. H., Crouse, J. D., Kjaergaard, H. G., and Wennberg, P. O.: New insights into  
280 the radical chemistry and product distribution in the OH-initiated oxidation of benzene, *Environ*  
281 *Sci Technol*, 54, 13467–13477, <https://doi.org/10.1021/acs.est.0c04780>, 2020.  
282